Microchimica Acta
https://doi.org/10.1007/s00604-019-3302-3

ORIGINAL PAPER

A voltammetric hybridization assay for microRNA-21 using carboxylated graphene oxide decorated with gold-platinum bimetallic nanoparticles

Anu Bharti[1] · Navneet Agnihotri[1] · Nirmal Prabhakar[1]

Received: 2 November 2018 / Accepted: 3 February 2019

Abstract

An electrochemical hybridization assay is described for the determination of microRNA-21. Fluorine tin oxide (FTO) sheets were coated with carboxylated graphene oxide followed by deposition of gold-platinum bimetallic nanoparticles by using chronoamperometry at a potential of −0.2 V for 350 s. The capture probe was immobilized on the surface of the modified FTO sheets by biotin-avidin interaction. On exposure to microRNA-21, hybridization occurs, and that can be detected at a relatively low working potential of 0.25 V by using ferri/ferro-cyanide as an electrochemical probe. The various modifications of the FTO sheets were characterized by means of FE-SEM, FT-IR, contact angle studies and electrochemical techniques. The effects of pH value, EDC-NHS activation time, concentration of capture probe and incubation time were optimized. The sensor has a wide linear response that extends from 1 fM to 1 μM of microRNA-21, and the detection limit is 1 fM. The sensor is stable for about 15 days (by retaining 90% of its initial activity) and can be reused for about 3 times (85% of initial activity) after regeneration with 50 mM NaOH solution. The sensor was applied to the analysis of spiked human serum and gave recoveries between 90 and 111%.

Keywords MicroRNA-21 · Breast Cancer · Electrochemical biosensor · Gene assay · Au-PtBNPs

Introduction

Breast cancer is the most common malignancy diagnosed among women worldwide. Frequently used biomarkers for breast cancer detection includes HER-2 [1], MUC1 [2] and CA15–3 [3] providing low sensitivity at primary stage diagnosis. Thus, there is an urgent need of diagnostic biomarker which can provide highly sensitive breast cancer detection at early stages.

MicroRNAs are highly conserved single stranded RNA molecules (19–22 nucleotides). They play a key role in post-transcriptional regulation of many biological processes like cell differentiation, proliferation and apoptosis [4]. Its aberrant expression is highly associated with occurrence and progression of various cancers like lung cancer [5], colorectal cancer [6] and breast cancer [7] etc. Circulating microRNAs are highly stable under different experimental conditions making them promising biomarker for diagnosis, prognosis and monitoring responses to many anti-cancerous therapies [8]. Some studies have proven microRNA-21 as suitable circulating and minimally invasive biomarker for breast cancer detection [9, 10]. Northern blotting and real time-polymerase chain reaction are the golden standards for microRNA's quantification and detection but are associated with some limitations. These methods are time consuming, expensive and require laborious procedures for microRNA extraction and purification. Therefore electrochemical biosensors are found to be suitable alternative device for early, sensitive and point-of-care diagnosis. The attractive features of electrochemical biosensors include quick response, ease of use, reusability, portability and low cost with number of available techniques like differential pulse voltammetry (DPV), cyclic voltammetry (CV), square wave voltammetry (SWV) and electrochemical impedance spectroscopy (EIS).

Nucleic acid probe based hybridization detection of microRNA-21 is preferred choice due to their high sensitivity and selectivity with better environmental stability. Many reports are available for detection of hybridization using electroactive indicators and monitoring of guanine oxidation current [11–13].

Electronic supplementary material The online version of this article (https://doi.org/10.1007/s00604-019-3302-3) contains supplementary material, which is available to authorized users.

✉ Nirmal Prabhakar
nirmalprabhakar@gmail.com; nirmalprabhakar@pu.ac.in

[1] Department of Biochemistry, Panjab University, Chandigarh 160014, India

Published online: 15 February 2019

Zhai and colleagues used a DNA based hybridization chain reaction amplification and streptavidin signal enhancement strategy for electrochemical detection of microRNA-21 [14]. The hairpin shaped capture DNA probe immobilized on gold electrode surface gets unfolded in the presence of target molecule triggering hybridization chain reaction amplification resulting in the formation of DNA double helix. The biosensor showed detection limit 0.56 fM for target microRNA-21 with high specificity. Miao and coworkers have also constructed an electrochemical biosensing platform for microRNA-21 detection using iridium (III) complex as catalyst [15]. The biosensor can detect microRNA-21 concentration as low as 1.6 fM over a detection range from 5 fM to 1 pM. A combination of biotinylated DNA/LNA molecular beacon probe and gold nanoparticles was used to create an integrated bio-recognition element to facilitate impedimetric detection of microRNA-21 [16]. A sandwich hybridization assays based on enzyme signal amplification have been reported for microRNA-21 determination using gold nanoparticles modified graphite pencil electrode [17]. Thiol terminated capture probe immobilized onto electrode surface by Au-S interaction was used to capture microRNA-21 with detection limit of 100 pM in a range from 200 pM to 388 nM. Su et al. employed a sandwich electrochemical assay by immobilizing thiolated DNA1 probe on the surface of gold nanoparticles-decorated MoS_2 nanosheet modified glassy carbon electrode [18]. The modified electrode surface was used to capture microRNA-21 and further incubated with DNA2 probe conjugated gold nanoparticles-decorated MoS_2 nanosheet. The biosensor detected microRNA-21 in a range from 10 fM to 1 nM with detection limit of 0.78 fM and 0.45 fM using DPV and EIS method, respectively. Researchers have also exploited methylene blue [19] and toludine blue [20] as redox indicators for hybridization based electrochemical detection of microRNA-21. Using pyrrolidinyl peptide nucleic acid/polypyrrole/silver nanofoam as electrode surface, a label free electrochemical microRNA-21 biosensor has been reported by Kangkamano et al. [21]. The sensor provided detection limit of 0.20 fM using CV method within 5 min of incubation time. Zhang et al. described a hybridization based impedance method for microRNA-21 detection [22]. This approach allowed the detection of target microRNA upto 4.3 fM using ZrO_2-reduced graphene oxide coated electrode coupled with catalytic hairpin assembly signal amplification strategy. A strand displacement reaction scheme was reported for microRNA-21 detection coupled with ferrocene as a signal molecule by Tian et al. [23]. N-carboxymethyl Chitosan/molybdenum carbide nanocomposite material deposited electrode surface was exploited in this strategy for microRNA-21 detection upto fM concentration. These electrochemical detection methods are combined with nanotechnology to enhance the sensitivity of biosensing platforms with improved electrolytic surface area. Further modifications and improvements may be done by reducing the number of hybridization steps.

Graphene oxide (GO) is having two dimensional structure with high surface area and capable of incorporating large amount of biomolecules on its surface due to the presence of many functional groups such as epoxy, hydroxyl and carboxyl on its basal plane and edges after modification compared to bare graphene [24]. Moreover, Graphene oxide provides many anchoring sites to bimetallic nanoparticles and reduces their tendency to aggregate. The carboxylated graphene oxide provides –COOH groups for covalent immobilization of various biomolecules. Bimetallic nanoparticles such as Au-PtBNPs are being extensively used due to their excellent electrical conductivity, catalytic activity, large electrochemical working window and stability in physical as well as chemical environment [25, 26]. Apart from this, gold nanoparticles exhibited great biocompatibility with platinum nanoparticles and provide better sensitivity for electrochemical biosensing in clinical samples [27]. Carboxylated graphene oxide (CGO) decorated with gold platinum bimetallic nanoparticles (Au-PtBNPs) provide better immobilization surface for biomolecules making it a significant biosensing platform. Here, we report the CGO decorated with Au-PtBNPs onto FTO electrode for immobilizing streptavidin and biotinylated capture probe for electrochemical detection of microRNA-21 based on its sequence complementarity.

Experimental

Chemicals and standard solutions

Graphite, chloroauric acid ($HAuCl_4$), chloroplatinic acid (H_2PtCl_6), streptavidin, 1-ethyl-3-(3-dimethylaminopropyl) carbodiimide (EDC), N-Hydroxysuccinimide (NHS), hydrogen peroxide (H_2O_2) and fluorine doped tin oxide (FTO) sheets were purchased from Sigma-Aldrich, USA (www.sigmaaldrich.com). Sodium dihydrogen orthophosphate ($NaH_2PO_4.2H_2O$) and di-sodium hydrogen orthophosphate anhydrous (Na_2HPO_4) were purchased from Thermo Fisher Scientific Pvt. Ltd., Mumbai, India (www.thermofisher.com). Chloroacetic acid, tris(hydroxymethyl)aminomethane (Tris), ethylenediaminetetraacetic acid (EDTA), potassium ferricyanide ($K_3Fe(CN)_6$) and potassium ferrocyanide trihydrate ($K_4Fe(CN)_6.3H_2O$) were received from HiMedia Laboratory Pvt. Ltd., Mumbai, India (www.himedialabs.com).

All the buffers employed in the study were as follows: TE buffer containing tris HCl (10 mM, pH 7.5) and EDTA (1 mM, pH 8.0) was used to prepare all the probe sequences. Phosphate buffer (PB) (50 mM, pH 7.0) was prepared by mixing Na_2HPO_4 (1.42 g) and $NaH_2PO_4.2H_2O$ (1.56 g) in 200 mL of dH_2O. 5 mM each of $K_3Fe(CN)_6$ and $K_4Fe(CN)_6.3H_2O$ was mixed in PB containing 0.9% NaCl. And the resulting $[Fe(CN)_6]^{3-/4-}$ solution was used as an electrolyte for carrying out all the electrochemical measurements.

All the probe sequences were procured from Sigma-Aldrich

Capture probe: 5′-[Btn]-TCA ACA TCA GTC TGA TAA GCT A-3'
Target probe (microRNA-21): 5'-UAG CUU AUC AGA CUG AUG UUG A-3'
One base mismatched microRNA-21: 5'-UAG AUU AUC AGA CUG AUG UUG A-3′
Two base mismatched microRNA-21: 5′-UAG GUU AUC AGA CUA AUG UUG A-3′
Non-target sequence (microRNA-155): 5'-UUA AUG CUA AUC GUG AUA GGG GU-3′

Apparatus and instrumentation

All the electrochemical measurements (CV, DPV and EIS) were performed using Autolab Potentiostat/Galvanostat [AutoLab 302NFRA32M] with three electrode system: a modified FTO electrode as working electrode, an Ag/AgCl as reference electrode and a platinum wire as counter electrode. The morphology of synthesized electrodes was examined by FE-SEM [Hitachi SU8000). FT-IR spectrum and contact angle measurements were recorded on [Nicolet 1S50 FT-IR] and Sessile drop [KRÜSS apparatus], respectively.

Synthesis of carboxylated graphene oxide (CGO)

GO was prepared according to the Hummer's method with some modifications [28]. In brief, a mixture containing 40 mL of concentrated H_2SO_4, 2 g of graphite powder and 1 g of $NaNO_3$ was kept at stirring for 1 h in an ice water bath. While stirring, 12 g of $KMnO_4$ was gradually added to above reaction mixture. After finishing the addition of $KMnO_4$, the mixture was removed from ice bath and heated at about 35 °C for half an hour. The reaction mixture was stirred at this temperature until a highly viscous solution is formed. The suspension was further treated with 200 mL of dH_2O and 40 mL of H_2O_2. The color of suspension changed from brownish to brilliant yellow. The suspension was centrifuged at 8000 rpm and sequentially washed with 5% HCl and water until pH of the supernatant reached to neutral. Finally, the synthesized GO was dried at 50 °C for 24 h in oven.

Carboxylation of GO was done under strongly basic conditions so as to convert hydroxyl moieties of GO into carboxyl groups using chloroacetic acid [29]. CGO was prepared by mixing 50 mg of GO powder, 1 g NaOH and 1.2 g chloroacetic acid into 100 mL of dH_2O, followed by ultrasonication for about 2 h. pH of the solution was adjusted to 7.4 with HNO_3 followed by several washings with acetone and water (1:1) using centrifugation. The final product was dried at 50 °C in oven.

Fabrication of Au-Pt bimetallic nanoparticles (Au-PtBNPs) and CGO on FTO electrode

Prior to use, FTO electrodes were thoroughly washed with 1% acetic acid solution, followed by acetone: ethanol (1:1) and dH_2O. Synthesized CGO was dissolved in 1% acetic acid (5 $mg.mL^{-1}$) by ultrasonic agitation for 1.5 h resulting in a homogenous black suspension. CGO modified FTO (CGO/FTO) electrode was prepared by drop casting a 15 μL aliquot of CGO suspension onto the surface of cleaned FTO electrode and dried overnight at room temperature. The CGO/FTO electrode was immersed in an electrochemical cell containing 1.0 mM $HAuCl_4$ and 1.0 mM H_2PtCl_6 with 0.2 M Na_2SO_4 and a constant potential of −0.2 V was applied for 350 s [30]. The electrode (Au-PtBNPs/CGO/FTO) was thoroughly rinsed with dH_2O.

Immobilization of capture probe

Streptavidin was attached to the surface of Au-PtBNPs/CGO/FTO electrode to ensure the immobilization of capture probe through biotin-avidin binding strategy. For this, EDC-NHS (5 mM EDC and 8 mM NHS in dH_2O) was incubated on the surface of electrode for 90 min to activate carboxylic moieties of CGO. Subsequently, streptavidin solution (0.05 $mg.mL^{-1}$ in PB) was incubated onto the Au-PtBNPs/CGO/FTO electrode surface, which covalently bind through amide linkage between its -NH_2 groups and -COOH groups of CGO. Then, biotinylated capture probe solution was dropped onto streptavidin modified Au-PtBNPs/CGO/FTO electrode and incubated overnight at 4 °C for drying. The CP/SA/Au-PtBNPs/CGO/FTO bioelectrode was then rinsed carefully with PB to remove any excess of unbound particles.

Characterization and optimization studies

The stepwise fabrication of FTO electrode was characterized by different techniques including FE-SEM, FT-IR, contact angle and electrochemical studies to affirm successful attachment of capture probe on its surface. CV studies of the modified electrodes were taken at potential range from (−0.6 to 1.2) V with scan rate of 50 mV/s. DPV measurements were taken within potential range from (0 to 0.8) V, step potential 0.02 V and modulation amplitude 0.1 V. EIS was taken within the frequency range from 100 kHz to 0.1 Hz at potential 10 mV.

To investigate the effect of various fabricated materials on electrode surface, CV responses were measured at different scan rates from 10 to 100 mV/s in 5 mM $[Fe(CN)_6]^3$

$^{-/4-}$solution. And the effective surface area is calculated in accordance with the Randles–Sevcik equation [31] (Table 1).

$$I_{pa} = 2.69 \times 10^5\ An^{3/2}C_oD_r^{1/2}\ v^{1/2} \quad (1)$$

Where, I_{pa} = anodic peak current, A = surface area of the electrode (cm^2).

n number of electrons participating in the redox reaction (1),
D_r diffusion coefficient (7.6×10^{-6} cm^2 s^{-1}).
C_0 concentration of $[Fe(CN)_6]^{3-/4-}$ (5 mol cm^{-3}).
v scan rate (V/s).

To achieve better response of microRNA-21 bioelectrode, various experimental parameters such as (a) pH of the supporting electrolyte, (b) EDC-NHS activation time, (c) concentration of capture probe to be immobilized and (d) incubation time required for target detection were optimized (Fig. S4). The details have been discussed in supplementary material. The pH of the supporting electrolyte (7.0) and EDC-NHS activation time (90 min) was selected for carrying out all the electrochemical measurements. 10 μM of probe concentration and 20 min of incubation time were selected for response studies.

Electrochemical detection of target hybridization

20 μL of the microRNA-21 solution was allowed to hybridize with CP/SA/Au-PtBNPs/CGO/FTO bioelectrode for 20 min followed by washing with PB. After washing the DPV measurements in 5 mM $[Fe(CN)_6]^{3-/4-}$ solution were taken to monitor the current change. The observed electrochemical signal was compared before and after hybridization and the resulting decrease in peak current after hybridization was proportional to microRNA-21 concentration. Different concentrations of microRNA-21 ranging from 1 fM to 1 μM were applied on electrode surface to evaluate limit of detection for microRNA-21. The protocol for stepwise modification of FTO electrode surface has been illustrated in Fig. 1.

Spike-in studies in human serum samples

The practical evaluation of this bioelectrode was also studied by spike-in varying concentration of microRNA-21 (1 fM, 10 fM, 100 fM, 1000 fM, 10,000 fM) in human serum samples.

Table 1 Effective surface area of different electrodes after modification

S. No.	Modified electrode surface	Effective surface area
1	CGO/FTO	0.243 cm^2
2	Au-PtBNPs/CGO/FTO	0.351 cm^2
3	SA/Au-PtBNPs/CGO/FTO	0.324 cm^2
4	CP/SA/Au-PtBNPs/CGO/FTO	0.270 cm^2

The spiked samples along with standard samples of same concentration were than subjected for DPV measurements using CP/SA/Au-PtBNPs/CGO/FTO bioelectrode for calculating the recovery percentage.

Results and discussion

Characterization of the modified electrodes

Contact angle The surface hydrophilicity of the electrodes was studied by sessile drop method (contact angle images are shown in Fig. S1). CGO is highly hydrophilic due to the presence of -COOH and -OH groups on its surface and showed contact angle of 30.1°. After applying Au-PtBNPs, contact angle increased (55.2°) due to the formation of hydrophobic layer. Contact angle of the electrode further decreased (38°) subsequently after the immobilization of streptavidin which may be attributed to the unique zwitter ionic composition with alternate $-NH_2$ and -COOH groups present in a peptide sequence [32]. Further, decrease in contact angle (15.2°) after applying capture probe sequence might be due to the influence of charged surface nucleic acid strands. These results confirm the successful formation of CP/SA/Au-PtBNPs/CGO/FTO bioelectrode.

FE-SEM images The surface morphology of various modified electrodes was examined by FE-SEM. Figure 2a shows the FE-SEM images of (i) CGO, (ii) Au-PtBNPs/CGO, (iii) SA/Au-PtBNPs/CGO and (iv) CP/SA/Au-PtBNPs/CGO deposited on the surface of FTO electrodes. CGO deposition over the surface of FTO electrode displays a thin wrinkled sheet-like appearance having minute edges (i) [33]. After the deposition of Au-PtBNPs, aggregates of cauliflower like structures is seen over CGO nanosheets (ii) [30]. The existence of carboxylic moieties on CGO/FTO electrode surface can provide better anchoring sites for streptavidin immobilization via CO-NH linkage. Figure 2a (iii) shows the attachment of streptavidin onto the Au-PtBNPs/CGO/FTO electrode with the appearance of large globules. The presence of streptavidin layer enables large amount of biotinylated-capture probe to get immobilized in a well dispersed manner which changed the morphological appearance of the SA/Au-PtBNPs/CGO/FTO electrode surface (iv). The electrode surface was also characterized by EDS mapping to confirm the successful deposition of Au-PtBNPs along with C and O atoms of CGO (Supplementary text 2, Fig. S2).

FT-IR The FT-IR spectrum of modified electrodes is shown in Fig. 2b confirming the presence of chemical bonds present in immobilized matrix due to surface modification steps. The CGO (i) shows strong peaks at 1720 cm^{-1} and 1030 cm^{-1} which are assigned to the C = O and C–O stretching vibrations of carboxylic group, respectively. Whereas, the peaks at 3280 cm^{-1}, 1550 cm^{-1} and 1380 cm^{-1} corresponds to the -

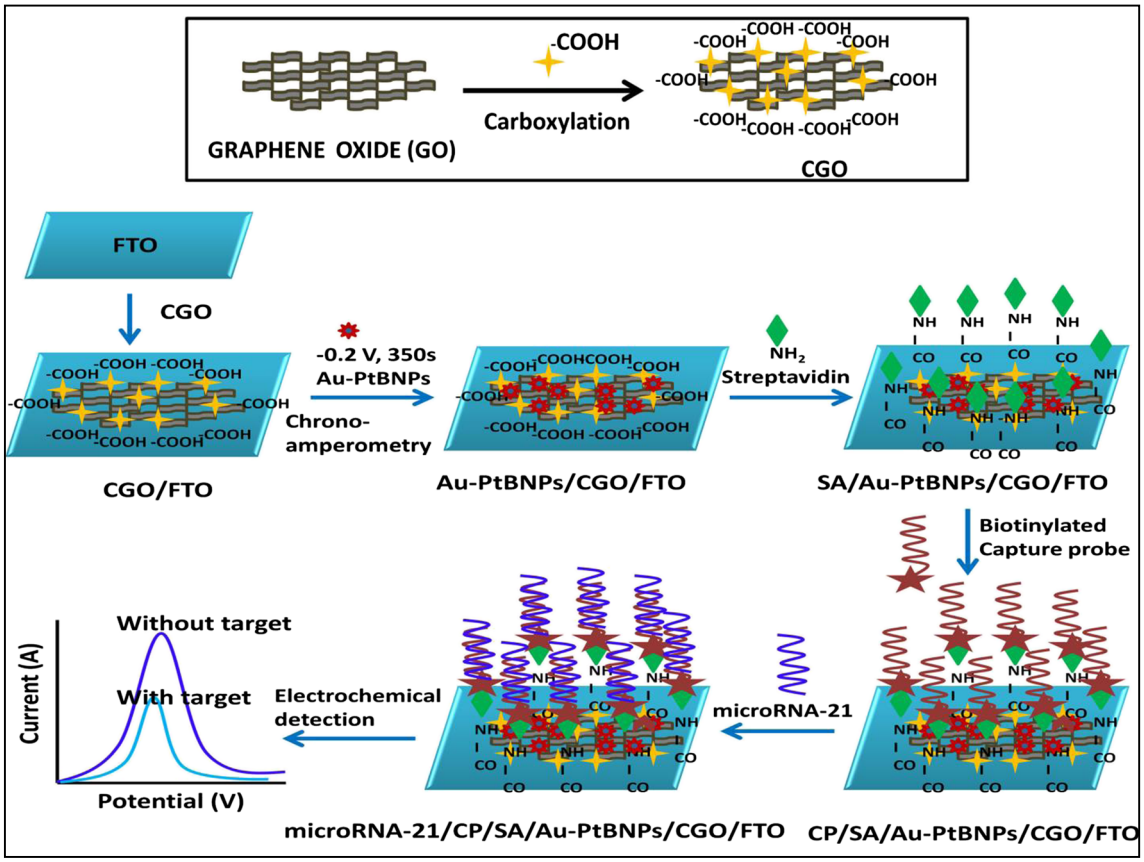

Fig. 1 Schematic illustration of electrode fabrication

OH (phenolic), C=C (aromatic) and O-H (hydroxyl) band stretching, respectively [34]. In the spectrum of Au-PtBNPs/CGO/FTO, only stretching vibrations of CGO are present, as Au-PtBNPs do not have any characteristic peak (ii). SA/Au-PtBNPs/CGO/FTO electrode shows intense peaks at 1630 cm^{-1} and 1580 cm^{-1} which can be attributed to the C=O stretch in amide I bond and N-H bend as well as C-N stretch in amide II bond due to the presence of streptavidin (iii) [35]. After coating capture probe sequence on SA/Au-PtBNPs/CGO/FTO electrode surface peaks at 1650 cm^{-1}, 1350 cm^{-1}, 1230 cm^{-1} and 1040 cm^{-1} appears (iv). The peaks at 1350 cm^{-1} and 1040 cm^{-1} can be ascribed to the C=C and C=N stretching of pyrimidine and purines bases. The peak at 1230 cm^{-1} indicates the presence of phosphate groups present in DNA strands [36]. Hence, FT-IR analysis confirmed the coordination of all the immobilized materials on CGO sheets.

Electrochemical characterization of modified electrodes

Cyclic voltammetry (CV), differential pulse voltammetry (DPV) and electrochemical impedance spectroscopy (EIS)

To investigate the electrochemical behavior of electrode fabrication, CV and DPV measurements were performed in 50 mM PB (pH -7.0, 0.9% NaCl) containing 5 mM $[Fe(CN)_6]^{3-/4-}$, at a scan rate of 50 mV/s. In Fig. 3a, a very small increase in the peak current (1.9×10^{-4} A) was observed in CGO (curve i). After the deposition of Au-PtBNPs on CGO surface (curve ii), an obvious increase in current response (5.8×10^{-4} A) was seen due to its highly conductive nature as well as excellent effective surface area to facilitate electron transfer at electrode surface. It may be concluded that CGO provide a better platform for biomolecule immobilization whereas Au-PtBNPs can improve the sensitivity of electrode by enhancing its current response. When streptavidin was immobilized on the surface of Au-PtBNPs/CGO/FTO electrode, current response decreased to 4.8×10^{-4} A (curve iii) due to the non-conducting nature of protein biomolecules. Current response further reduced to 4.3×10^{-4} A after applying capture probe sequence (curve iv). It can be ascribed to the presence of negatively charged DNA backbone which can block the flow of electrons from negatively charged $[Fe(CN)_6]^{3-/4-}$ solution. Subsequently, as target microRNA-21 hybridized with capture probe, the current response further decreased to 3.7×10^{-4} A (curve v) due to the loading of more negative charges on electrode surface. To further validate the results the electrodes were also subjected to DPV studies (Fig. 3a inset) and the current responses are in agreement with CV results.

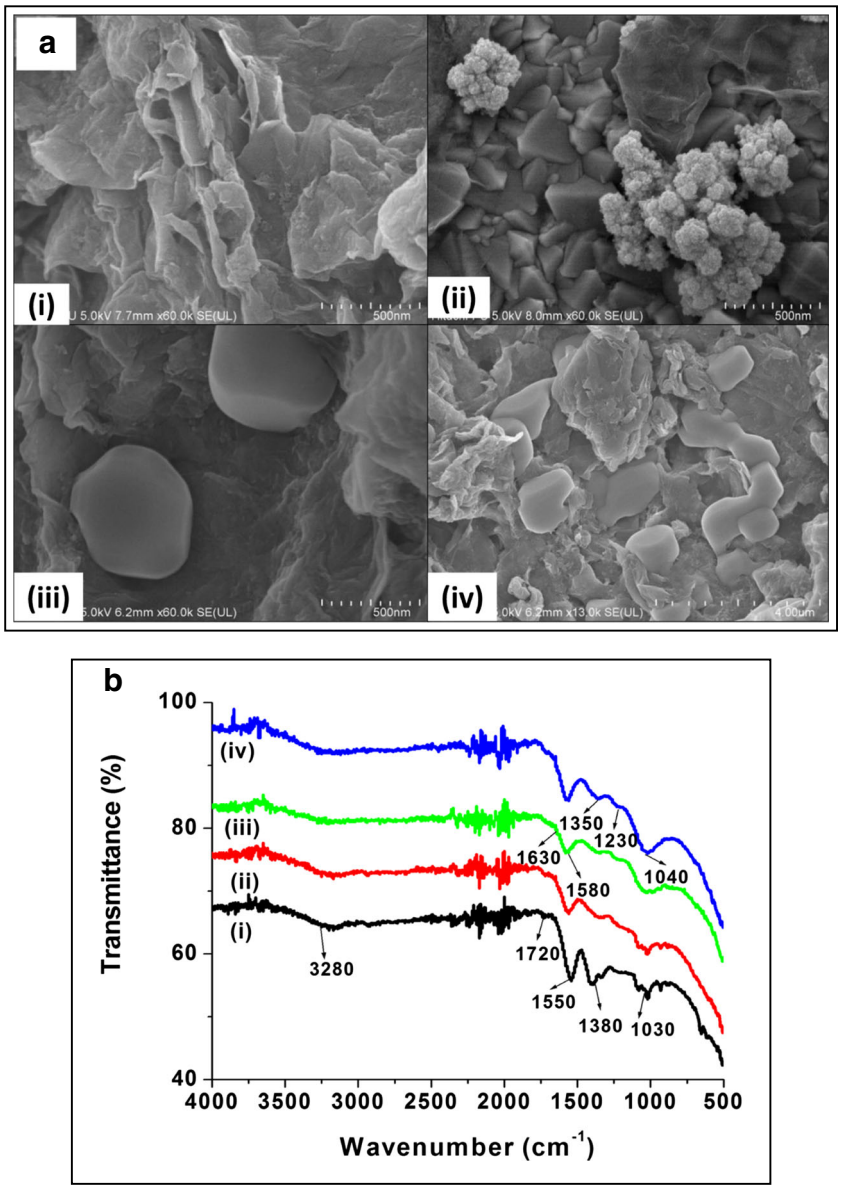

Fig. 2 **a** FE-SEM images and **b** FT-IR spectra for step wise modification of (i) CGO/FTO, (ii) Au-PtBNPs/CGO/FTO, (iii) SA/Au-PtBNPs/CGO/FTO and (iv) CP/SA/Au-PtBNPs/CGO/FTO

Figure 3b shows EIS results of these electrodes performed in 50 mM PB (pH -7.0, 0.9% NaCl) containing 5 mM $[Fe(CN)_6]^{3-/4-}$. Nyquist plot measures the impedance changes occurring on the FTO electrode surface during various modifications. The diameter of semicircle indicates higher electron transfer resistance of the CGO immobilized FTO electrode (curve i). After electrodeposition of Au-PtBNPs, semicircle is not formed and electrode exhibits almost straight line attributing to its high electron transfer capacity (curve ii). Furthermore, the electron transfer capacity decreased after applying streptavidin (curve iii), capture probe (curve iv) and microRNA-21 (curve v) on to the electrode surface resulting in the formation of semicircle like appearance from the straight line. The results clearly demonstrate that the CGO decorated with Au-PtBNPs nanocomposite based matrix is highly conductive and can be used for further study.

Effective surface area

It is noted from Fig. 3c that oxidation peak current increases and shifts towards the positive potential with the increasing scan rate. The peak current is proportional to the square root of scan rates and the slope was used to calculate the effective surface area of modified electrodes as given in Table 1. The enhancement in the effective surface area of electrode after Au-PtBNPs deposition makes it a suitable fabrication platform for biosensor development.

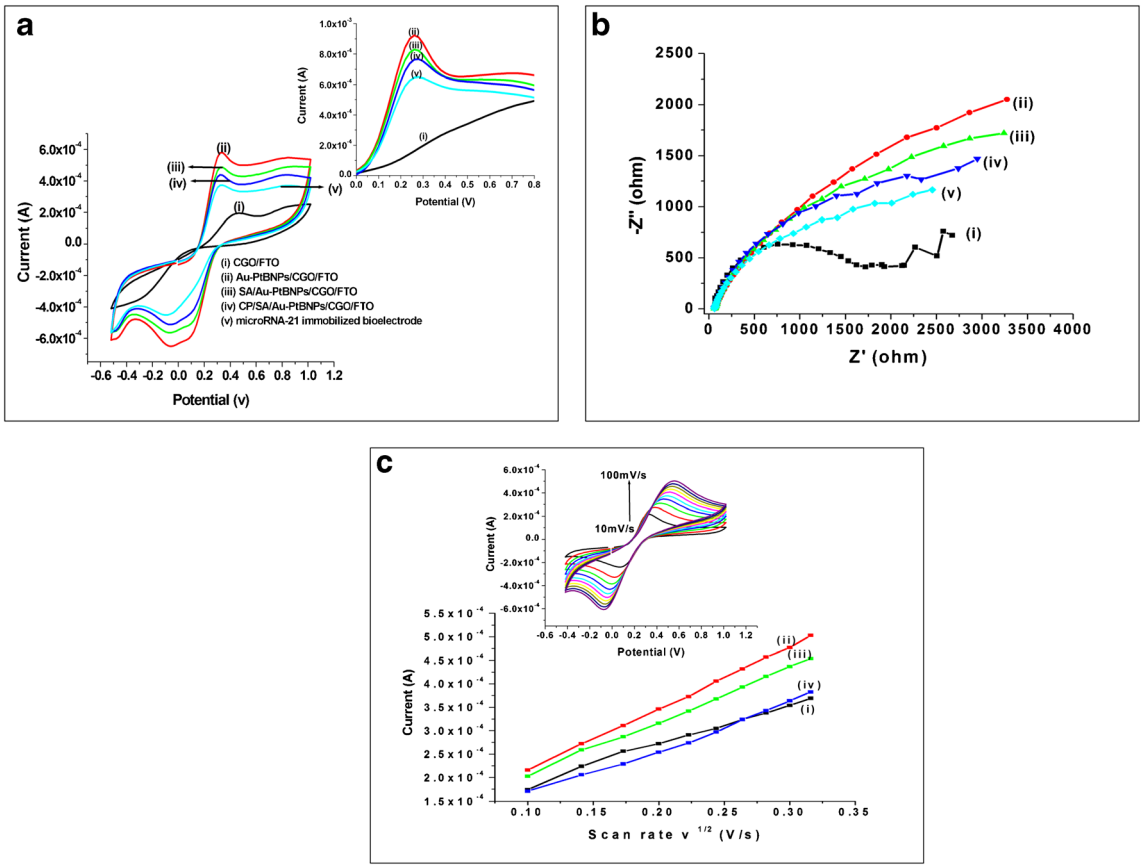

Fig. 3 Electrochemical studies: **a** CV & DPV (inset) **b** EIS of (i) CGO, (ii) Au-PtBNPs/CGO, (iii) SA/Au-PtBNPs/CGO, (iv) CP/SA/Au-PtBNPs/CGO, and (v) microRNA-21 hybridized CP/SA/Au-PtBNPs/CGO coated FTO electrode in 50 mM PB (pH -7.0, 0.9% NaCl) containing 5 mM $[Fe(CN)_6]^{3-/4-}$. **c** Slope of the CV responses of above mentioned electrodes measured at different scan rates from 10 to 100 mV/s in 5 mM $[Fe(CN)_6]^{3-/4-}$ solution

Analytical performance

Under optimized experimental conditions, a range of microRNA-21concentration (1 fM-1 μM) was analyzed by CP/SA/Au-PtBNPs/CGO/FTO bioelectrode in $[Fe(CN)_6]^{3-/4-}$ solution using DPV (Fig. 4a). The current response of the bioelectrode decreased after interaction with the increasing concentration of microRNA-21 within the range of 1 fM-1 μM. The results depict that the formation of hybridization complex between capture probe and target microRNA inhibits the electron flow leading to significant decrease in current. The least detected concentration of microRNA-21 is 1 fM, below this concentration the current value of the bioelectrode was similar to base electrode (un-hybridized CP/SA/Au-PtBNPs/CGO/FTO). A plot of change in current response with increasing microRNA concentration is given in Fig. 4b, Inset represents a calibration plot, showing linear relationship between the change in peak current and log of microRNA-21 concentration with regression equation as

$$Y = -5.72 \times 10^{-5}X + 0.0011 \text{ (Correlation coefficient} = -0.9977) \quad (2)$$

where, X is log of microRNA-21 concentration (fM) and Y is DPV peak current (A).

Additionally, the sensitivity of our method is also compared with previously reported methods in Table 2.

Specificity, stability and reusability studies

The specificity, stability and reusability studies of the CP/SA/Au-PtBNPs/CGO/FTO bioelectrode were performed in triplicate using 50 mM PB (pH -7.0, 0.9% NaCl) containing 5 mM $[Fe(CN)_6]^{3-/4-}$ (Fig. 5). To investigate the specificity of bioelectrode, the electrochemical response of some interferents like one base mismatch, two base mismatch, non-target (miRNA-155) and their mixture (with a concentration of 100 nM) was compared with the target microRNA-21. There was no significant change in the current value of CP/SA/Au-PtBNPs/CGO/FTO after incubation with all the interferents (Fig. 5a). The current value was almost equal to the current value observed in bare bioelectrode. However, there was decrease in the current value when incubated with mixture of interferents due to hybridization with microRNA-21 present in mixture. Hence, it can

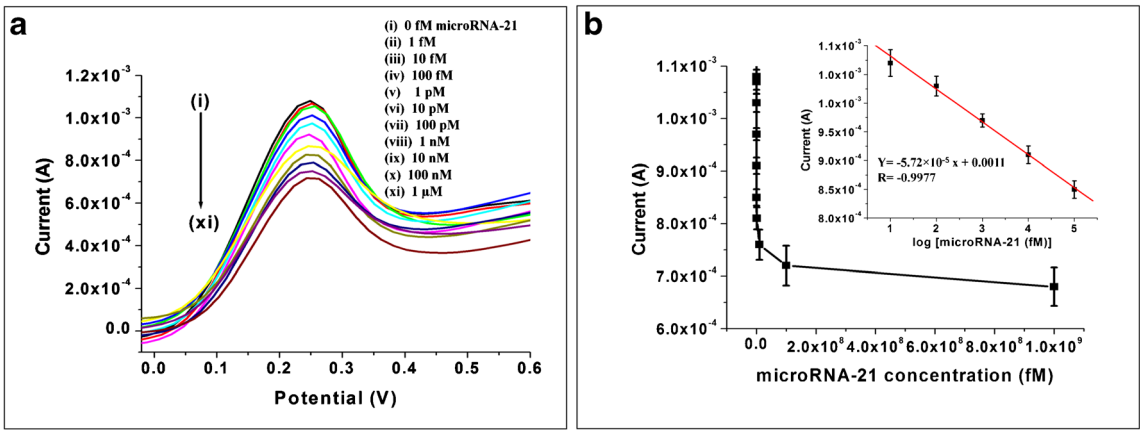

Fig. 4 **a** DPV response of different concentrations of microRNA-21 (i) 0 fM (ii) 1 fM (iii) 10 fM (iv) 100 fM (v) 1 pM (vi) 10 pM (vii) 100 pM (viii) 1 nM (ix) 10 nM (x) 100 nM (xi) 1 μM, incubated on CP/SA/Au-PtBNPs/CGO coated FTO electrode using 50 mM PB (pH -7.0, 0.9% NaCl) containing 5 mM $[Fe(CN)_6]^{3-/4-}$. **b** The plot of changes in current responses with increasing microRNA-21 concentration from 1 fM to 1×10^9 fM. Inset shows calibration plot between current responses and log of linear microRNA-21 concentration. (Error bars represent standard deviation of three independent experiments)

be concluded that CP/SA/Au-PtBNPs/CGO/FTO bioelectrode is highly specific for microRNA-21.

To evaluate the stability, CP/SA/Au-PtBNPs/CGO/FTO bioelectrode was stored at 4 °C for about a month and DPV response was measured at an interval of 5 days. It can be seen from Fig. 5b, that the bioelectrode exhibited 98%, 94%, 90%, 87%, 83% and 81% of its initial current response at 5th, 10th, 15th, 20th, 25th and 30th day of storage, respectively.

The reusability of the bioelectrode was evaluated by repetitive detection of microRNA-21 in optimized conditions. After each detection, the electrode was regenerated by incubating with 50 mM NaOH solution for 10 min to dissociate microRNA and capture probe duplex from electrode surface followed by washing in PB. The regenerated bioelectrode was further used for electrochemical detection of microRNA-21. The current response of first detection was taken as 100% and subsequent detections showed 96%, 90%, 85%, 77%, 72%, 68%, 65% and 61% of original current signal (Fig. 5c). The results indicated that this bioelectrode has good stability for microRNA-21 detection upto 15 days (90% of initial value) and can be reused for about 3 times (with 85% of initial value).

Table 2 Comparison of different electrodes for the determination of microRNA-21 on the basis of their analytical features

Biosensing platform	Detection method	Linear range	Detection limit	Response time	Ref.
[a]microRNA-21/BSA/MCH/CP/AuE	DPV	1 fM-100 pM	0.56 fM	60 min	[14]
[b]Iridium (III) complex/DP-AuNPs /microRNA-21/CP/AuE	CV	5.0 fM- 1.0 pM	1.6 fM	30 min	[15]
[c]Biotin-MB-AuNPs	EIS	1 pM-1 nM	0.3 pM	60 min	[16]
[d]SA-ALP/B-P2/T/MCH/SH-P1/AuNPs/PGE	DPV	200 pM- 388 nM	100 pM	35 min	[17]
[e]DNA2AuNPs@MoS_2/microRNA-21/MCH/DNA1/AuNPs@MoS_2/-GCE	DPV EIS	10 fM-1 nM	0.78 fM 0.45 fM	–	[18]
[f]ssDNA probe/MWCNT-COOH/GCE	DPV	0.1–500 pM	84.3 fM	30 min	[19]
[g]TB/microRNA-21/ssRNA/AuNS/GCE	DPV	100 aM-1 nM	78 aM	60 min	[20]
[h]acpcPNA/PPy/AgNF/AuE	CV	0.2 fM-1 nM	0.2 fM	5 min	[21]
[i]H2/H1/PAA/ZrO_2-RGO/GCE	EIS	10 fM-100 pM	4.3 fM	50 min	[22]
[j]HDNA1 & HDNA2-Fc/p-DNA/ Mo_2C nanosheet/NCS/GCE	Amperometric (i-t)	1 fM-1 nM	0.34 fM	90 min	[23]
CP/SA/Au-PtBNPs/CGO/FTO	DPV	1 fM-1 μM	1 fM	20 min	Present work

Abbreviations: [a] BSA-bovine serum albumin; MCH- 6-mercapto-1-hexanol; CP- capture probe; AuE- Au electrode; [b] DP- DNA probe; [c] MB- molecular beacon; [d] SA-ALP- streptavidin-conjugated alkaline phosphatase; B-P2- biotin labeled probe 2; T-target microRNA; SH-P1- thiol terminated capture probe 1; PGE- pencil graphite electrode [e] AuNPs@MoS2- gold nanoparticles- decorated MoS_2 nanosheets; DNA1 & DNA2- probe DNA; GCE- glassy carbon electrode; [f] ssDNA-single stranded DNA; MWCNT- multiwalled carbon nanotubes; [g] TB- toluidine blue; ssRNA- single stranded RNA; AuNS-AuNPs superlattice; [h] acpcPNA- peptide nucleic acid derived from a D-prolyl-2-aminocyclopentanecarboxylic acid backbone; PPy- polypyrroleAgNF-silver nanofoam; [i] H1 & H2- hairpin DNA molecules; PAA- poly(acrylic acid); RGO- reduced graphene oxide; [j] HDNA1 & HDNA2-Fc- hairpin DNA-ferrocene; p-DNA- probe DNA; Mo_2C- molybdenumcarbide; NCS- N-carboxymethyl chitosan

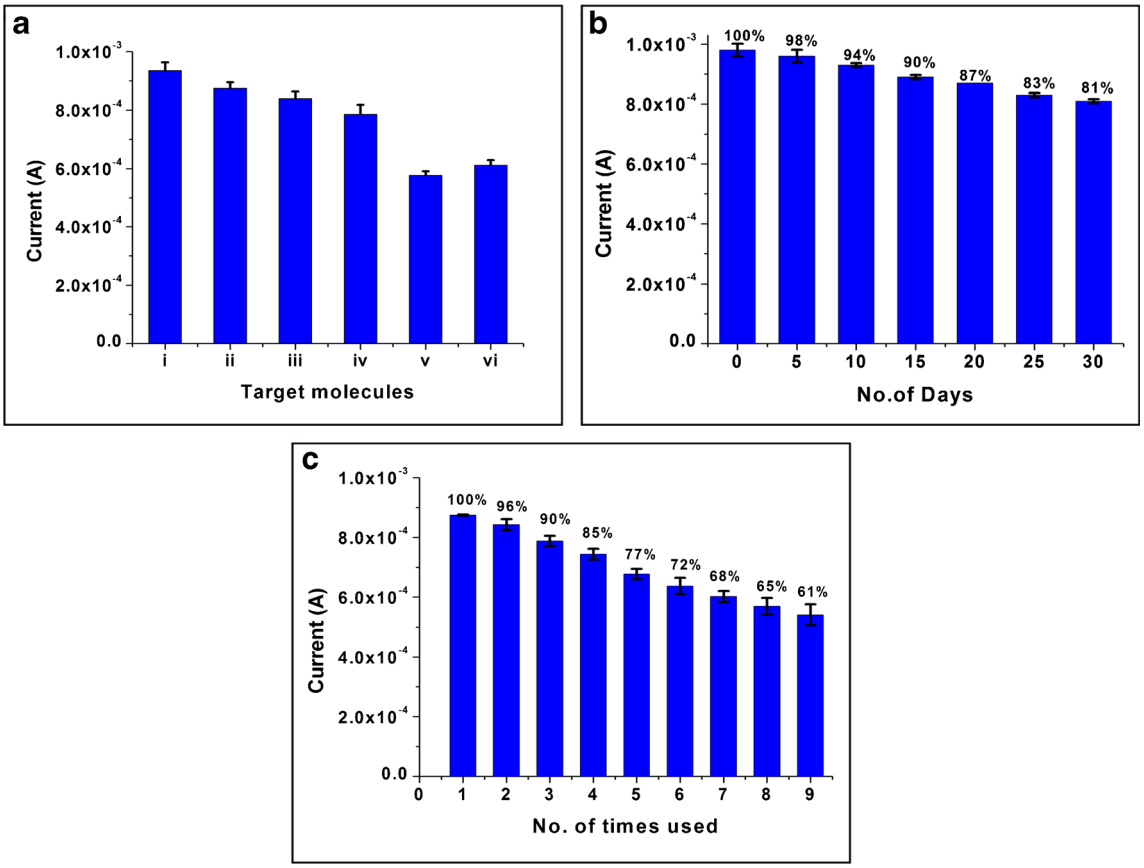

Fig. 5 **a** Selectivity of CP/SA/Au-PtBNPs/CGO/FTO bioelectrode against other interferents: (i) Blank (ii) miRNA-155 (iii) One base mismatch (iv) Two base mismatch (v) microRNA-21 and (vi) Mixture solution, **b** Stability of the bioelectrode for 30 days at an interval of 5 days incubated at 4 °C and **c** Reusability studies of the bioelectrode. (Error bars represent standard deviation of three independent bioelectrodes)

Reproducibility

The reproducibility was also examined by DPV measurements by incubating two different target concentrations (10 pM and 100 pM) on CP/SA/Au-PtBNPs/CGO/FTO surface. Two sets of five different electrodes were evaluated on the same day using 10 pM and 100 pM of microRNA-21 for intra assay. While for inter assay, other two sets of five electrodes were used to sense both the concentration for five subsequent days. The electrochemical responses were found to be similar for all the electrodes with same target concentration (Fig. S5). The relative standard deviation was determined to be 2.3% and 2.1% for intra assay (same day) whereas 2.1% and 2.5% for inter assay (on next subsequent days), in case of 10 pM as well as 100 pM, respectively. The above results demonstrate acceptable reproducibility of the bioelectrode.

Table 3 Determination of microRNA-21 in spiked serum samples ($n = 3$) using CP/SA/Au-PtBNPs/CGO/FTO bioelectrode

Sample	Added (fM)	Found (fM)	Recovery (%)
1	1	0.993	99.3 ± 5.5
2	10	9.08	90.8 ± 6.1
3	100	102	102 ± 4.9
4	1000	932	93.2 ± 5.8
5	10,000	11,155	111.5 ± 12.4

(±denotes relative standard deviation)

Spike-in studies

Table 3 illustrates % recovery of the bioelectrode for spiked human serum samples with microRNA-21 concentration ranging from 1 fM to 10 pM. The bioelectrode exhibited recovery from 90 to 111.5% and relative standard deviation ranging from 4.9 to 12.4%. Hence, it can be used for the determination of microRNA-21 in real samples.

Conclusion

Au-Pt bimetallic nanoparticles were decorated onto CGO coated FTO sheets for the development of electrochemical bioelectrode for rapid, simple and sensitive measurement of microRNA-21 as a biomarker for breast cancer. Owing to the large surface area of GO with carboxylic moieties and increased electrical conductivity of bimetallic nanoparticles,

the capture probe immobilized on SA/Au-PtBNPs/CGO/FTO bioelectrode resulted in sensitive and specific hybridization with complementary target microRNA-21. The CP/SA/Au-PtBNPs/CGO/FTO based biosensor allowed detection of microRNA-21 upto1 fM with good reproducibility and stability which proved it a promising platform for point-of-care diagnosis of breast cancer in clinical applications. The bioelectrode can effectively discriminate other interferents from microRNA-21 showing good selectivity. The present strategy offers convenient procedures for biomedical research as it can be applied for the analysis of other cancer related biomolecules.

Acknowledgements This work was financially supported by Department of Science and Technology [DST-Purse II], Special Assistance Programme (UGC-SAP) [F.4-7/2015/DRS-III (SAP-II)] and DST-SERB sponsored project [EEQ/2017/000239]. Council of Scientific & Industrial Research (CSIR) is highly acknowledged for the award of SRF [09/135(0729)/2016-EMR-I]. Authors also acknowledge Central Instrument Laboratory (CIL) facility of Panjab University, Chandigarh for FE-SEM studies. We are thankful to Dr. Shweta Rana (Department of Chemistry, Panjab University, Chandigarh) and Dr. Suman Singh (Central Scientific Instruments Organisation (CSIR-CSIO), Chandigarh) for their support in performing FT-IR and Contact angle studies, respectively.

Compliance with ethical standards The authors declare that they have no competing interests.

References

1. Chun L, Kim SE, Cho M, Choe WS, Nam J, Lee DW, Lee Y (2013) Electrochemical detection of HER2 using single stranded DNA aptamer modified gold nanoparticles electrode. Sensors Actuators B Chem 186:446–450
2. Gupta P, Bharti A, Kaur N, Singh S, Prabhakar N (2018) An electrochemical aptasensor based on gold nanoparticles and graphene oxide doped poly(3,4-ethylenedioxythiophene) nanocomposite for detection of MUC1. J Electroanal Chem 813:102–108
3. Chang CC, Chiu NF, Lin DS, Chu-Su Y, Liang YH, Lin CW (2010) High-sensitivity detection of carbohydrate antigen 15-3 using a gold/zinc oxide thin film surface Plasmon resonance-based biosensor. Anal Chem 82:1207–1212
4. Mattick JS, Makunin IV (2006) Non-coding RNA. Hum Mol Genet 15:R17–R29
5. Leng QX, Lin YL, Jiang FR, Lee CJ, Zhan M, Fang HB, Wang Y, Jiang F (2017) A plasma miRNA signature for lung cancer early detection. Oncotarget 8:111902–111911
6. Lanza G, Ferracin M, Gafa R, Veronese A, Spizzo R, Pichiorri F, Liu CG, Calin GA, Croce CM, Negrini M (2007) mRNA/microRNA gene expression profile in microsatellite unstable colorectal cancer. Mol Cancer 6:54
7. Xin FX, Li M, Balch C, Thomson M, Fan MY, Liu Y, Hammond SM, Kim S, Nephew KP (2009) Computational analysis of microRNA profiles and their target genes suggests significant involvement in breast cancer antiestrogen resistance. Bioinformatics 25:430–434
8. McGuire A, Brown JAL, Kerin MJ (2015) Metastatic breast cancer: the potential of miRNA for diagnosis and treatment monitoring. Cancer Metastasis Rev 34:145–155
9. Lowery AJ, Miller N, McNeill RE, Kerin MJ (2008) MicroRNAs as prognostic indicators and therapeutic targets: potential effect on breast cancer management. Clin Cancer Res 14:360–365
10. Chan M, Liaw CS, Ji SM, Tan HH, Wong CY, Thike AA, Tan PH, Ho GH, Lee ASG (2013) Identification of circulating microRNA signatures for breast cancer detection. Clin Cancer Res 19:4477–4487
11. Lusi EA, Passamano M, Guarascio P, Scarpa A, Schiavo L (2012) Innovative electrochemical approach for an early detection of microRNAs. Anal Chem 81:2819–2822
12. Kilic T, Topkaya SN, Ariksoysal DO, Ozsoz M, Ballar P, Erac Y, Gozen O (2012) Electrochemical based detection of microRNA, mir21 in breast cancer cells. Biosens Bioelectron 38:195–201
13. Liu LZ, Song C, Zhang Z, Yang J, Zhou LL, Zhang X, Xie GM (2015) Ultrasensitive electrochemical detection of microRNA-21 combining layered nanostructure of oxidized single-walled carbon nanotubes and nanodiamonds by hybridization chain reaction. Biosens Bioelectron 70:351–357
14. Zhai Q, He Y, Li XL, Guo J, Li SQ, Yi G (2015) A simple and ultrasensitive electrochemical biosensor for detection of microRNA based on hybridization chain reaction amplification. J Electroanal Chem 758:20–25
15. Miao XM, Wang WH, Kang TS, Liu JB, Shiu KK, Leung CH, Ma DL (2016) Ultrasensitive electrochemical detection of miRNA-21 by using an iridium(III) complex as catalyst. Biosens Bioelectron 86:454–458
16. Azzouzi S, Mak WC, Kor K, Turner APF, Ben Ali M, Beni V (2017) An integrated dual functional recognition/amplification bio-label for the one-step impedimetric detection of micro-RNA-21. Biosens Bioelectron 92:154–161
17. Mandli J, Mohammadi H, Amine A (2017) Electrochemical DNA sandwich biosensor based on enzyme amplified microRNA-21 detection and gold nanoparticles. Bioelectrochemistry 116:17–23
18. Su S, Cao WF, Liu W, Lu ZW, Zhu D, Chao J, Weng LX, Wang LH, Fan CH, Wang LH (2017) Dual-mode electrochemical analysis of microRNA-21 using gold nanoparticle-decorated MoS2 nanosheet. Biosens Bioelectron 94:552–559
19. Rafiee-Pour HA, Behpour M, Keshavarz M (2016) A novel label-free electrochemical miRNA biosensor using methylene blue as redox indicator: application to breast cancer biomarker miRNA-21. Biosens Bioelectron 77:202–207
20. Tian L, Qian K, Qi J, Liu QY, Yao C, Song W, Wang YH (2018) Gold nanoparticles superlattices assembly for electrochemical biosensor detection of microRNA-21. Biosens Bioelectron 99:564–570
21. Kangkamano T, Numnuam A, Limbut W, Kanatharana P, Vilaivan T, Thavarungkul P (2018) Pyrrolidinyl PNA polypyrrole/silver nanofoam electrode as a novel label free electrochemical miRNA-21 biosensor. Biosens Bioelectron 102:217–225
22. Zhang KY, Zhang N, Zhang L, Wang HY, Shi HW, Liu Q (2018) Label-free impedimetric sensing platform for microRNA-21 based on ZrO2-reduced graphene oxide nanohybrids coupled with catalytic hairpin assembly amplification. RSC Adv 8:16146–16151
23. Tian L, Qi JX, Ma XY, Wang XJ, Yao C, Song W, Wang YH (2018) A facile DNA strand displacement reaction sensing strategy of electrochemical biosensor based on N-carboxymethyl chitosan/molybdenum carbide nanocomposite for microRNA-21 detection. Biosens Bioelectron 122:43–50
24. Dreyer DR, Park S, Bielawski CW, Ruoff RS (2010) The chemistry of graphene oxide. Chem Soc Rev 39:228–240
25. Li Z, An ZZ, Guo YY, Zhang KN, Chen XL, Zhang DX, Xue ZH, Zhou XB, Lu XQ (2016) Au-Pt bimetallic nanoparticles supported

on functionalized nitrogen-doped graphene for sensitive detection of nitrite. Talanta 161:713–720
26. Ghani M, Masoum S, Ghoreishi SM (2018) Three-dimensional Pd/Pt bimetallic nanodendrites on a highly porous copper foam fiber for headspace solid-phase microextraction of BTEX prior to their quantification by GC-FID. Microchim Acta 185:527
27. Jain U, Gupta S, Chauhan N (2017) Construction of an amperometric glycated hemoglobin biosensor based on au–Pt bimetallic nanoparticles and poly (indole-5-carboxylic acid) modified au electrode. Int J Biol Macromol 105:549–555
28. Lee CY, Van Le Q, Kim C, Kim SY (2015) Use of silane-functionalized graphene oxide in organic photovoltaic cells and organic light-emitting diodes. Phys Chem Chem Phys 17:9369–9374
29. Peng SG, Liu CY, Fan XJ (2015) Surface modification of graphene oxide by carboxyl-group: preparation, characterization, and application for proteins immobilization. Integr Ferroelectr 163:42–53
30. Yang T, Zhou N, Li QH, Guan Q, Zhang W, Jiao K (2012) Highly sensitive electrochemical impedance sensing of PEP gene based on integrated au-Pt alloy nanoparticles and polytyramine. Colloids Surf B: Biointerfaces 97:150–154
31. Thakur H, Kaur N, Sabherwal P, Sareen D, Prabhakar N (2017) Aptamer based voltammetric biosensor for the detection of mycobacterium tuberculosis antigen MPT64. Microchim Acta 184:1915–1922
32. Cui M, Wang Y, Wang HP, Wu YM, Luo XL (2017) A label-free electrochemical DNA biosensor for breast cancer marker BRCA1 based on self-assembled antifouling peptide monolayer. Sensors Actuators B Chem 244:742–749
33. Wen W, Huang JY, Bao T, Zhou J, Xia HX, Zhang XH, Wang SF, Zhao YD (2016) Increased electrocatalyzed performance through hairpin oligonucleotide aptamer-functionalized gold nanorods labels and graphene-streptavidin nanomatrix: highly selective and sensitive electrochemical biosensor of carcinoembryonic antigen. Biosens Bioelectron 83:142–148
34. Yu S, Liu J, Zhu W, Hu ZT, Lim TT, Yan X (2015) Facile room-temperature synthesis of carboxylated graphene oxide-copper sulfide nanocomposite with high photodegradation and disinfection activities under solar light irradiation. Sci Rep 5:16369
35. Lapin NA, Chabal YJ (2009) Chabal, infrared characterization of biotinylated silicon oxide surfaces, surface stability, and specific attachment of streptavidin. J Phys Chem B 113:8776–8783
36. Banyay M, Sarkar M, Graslund A (2003) A library of IR bands of nucleic acids in solution. Biophys Chem 104:477–488